Research Paper

Analytical and Computational Acoustic Modelling of Side Outlet Muffler and Its Extension in the Modelling of Tapered Side Outlet Muffler

Sandeep Kumar VISHWAKARMA, Suryappa Jayappa PAWAR*

Department of Applied Mechanics, Motilal Nehru National Institute of Technology Allahabad
Prayagraj, India

*Corresponding Author e-mail: sjpawar@mnnit.ac.in

Mufflers are popular in the suppression of noise levels coming from various machinery. The most common parameters for the evaluation of the performance of mufflers are transmission loss, noise level, and insertion loss. The transmission loss is evaluated for tapered side outlet muffler using finite element analysis without considering the fluid-structure interaction. This study includes analytical modelling and acoustic modelling of the side outlet muffler and transmission loss is in excellent agreement with the reference paper. The feasibility of the acoustic model is also verified with the experimental work on simple expansion chamber muffler. The same finite element analysis is extended for the tapered side outlet muffler. The transmission loss of the tapered side outlet muffler in the given frequency range is found 8.96 dB better than the side outlet muffler. The acoustic pressure level and sound pressure level contours for the tapered side outlet muffler give a clear picture of wave propagation inside the muffler. The effect of the cut-off frequency on the transmission loss of the tapered side outlet muffler can be seen from the contours. This study can be helpful in the determination of the performance of the mufflers in terms of transmission loss, the performance of mufflers above cut-off frequency, and design improvements in the muffler to avoid the higher-order modes of the sound wave.

Keywords: 1-D analysis; FEA; sound pressure level; transfer matrix; transmission loss.

1. Introduction

The traditional reactive mufflers use different expansion chambers for noise suppression. The expansion chambers introduce discontinuity in the shape of the muffler. The discontinuities in mufflers, such as sudden area expansion, duct extensions, sudden area contraction, etc. result in extra impedances causing impedance mismatch. The impedance mismatch is the basis for the reactive mufflers for their operation. The principle of noise cancellation of conventional mufflers is presented in the literature (BANERJEE, JACOBI, 2013; 2015; KESKAR, VENKATESHAM, 2017; MIMANI, MUNJAL, 2016; KANI et al., 2019; PERREY-DEBAIN et al., 2014). The transfer matrix method is well-known and very elementary in any textbook based on acoustics or muffler design (WU et al., 1998; SEYBERT, CHENG, 1987; WU, WAN, 1996). MUNJAL (1975) and TO (1984) used the 4-pole method for the prediction of the performance of mufflers. LAMANCUSA (1988) de-

rived the coefficient of transmission loss for several cases of double expansion chambers. SUWANDI et al. (2005) proposed the plane wave transmission line principle to calculate the transmission loss of different cases of mufflers.

The analytical methods developed earlier for the investigation of mufflers are valid for plane waves only (MUNJAL, 1987). The higher-order modes of the wave inside the muffler cannot be analyzed with the analytical methods (ÅBOM, 1990). This limitation of analytical methods can be eliminated with the help of 3-D analytical techniques and computational techniques. SELAMET and JI (1998) proposed a 3-D analytical method for the mufflers having offset inlet and outlet to study the effect of multidimensional wave propagation on the effectiveness of mufflers. The finite element analysis (FEA) is the most popular computational technique for the acoustic analysis of mufflers. The FEA was first applied by YOUNG and CROCKER (1975) for a simple expansion chamber muffler. KAGAWA

and OMOTE (1976) performed FEA for circular cross-section mufflers but failed to predict the performance of complex mufflers. CRAGGS (1989) analysed a rectangular duct system with a 3-D FEA and reduced the system size resulting in a low computational memory requirement. SAHARABUDHE *et al.* (1991) used the sub-structuring principle along with the matrix condensation technique to analyse expansion chamber mufflers using 3-D finite elements. BILAWCHUK and FYFE (2003) compared different modelling methods for mufflers and concluded that FEA was the best among the methods. The FEA also plays an important role in the shape optimization (CHANG *et al.*, 2004; CHANG, CHIU, 2010; CHIU, 2011) of the mufflers (BARBIERI, BARBIERI, 2006; KUSKINEN *et al.*, 2010; CHANG *et al.*, 2018). MIMANI and MUNJAL (2012) analyzed an elliptical-shaped silencer with an end inlet and side outlet using an impedance matrix approach. The effects of port locations, and the chamber length on the transmission loss of elliptical chamber muffler were presented. A comparison of circular and elliptic chambers was also presented and results were compared with FEA.

In the present study, the acoustic modelling of a tapered side outlet muffler was done. Initially, the analytical modelling of a side outlet muffler with a straight expansion chamber was done and the transmission loss of the muffler was compared and validated with (ZHANG *et al.*, 2020) and with a maximum percentage error of 0.016%. Further, the acoustic modelling of the side outlet muffler with a straight expansion chamber was also done using FEA. The grid independency test is done by taking transmission loss as the parameter. The transmission loss of the side outlet muffler from FEA is compared and validated with (ZHANG *et al.*, 2020) and the maximum percentage error found is 0.19%, which is well under the acceptable range. This FEA model is also verified with the experimental work on simple expansion chamber muffler (TAO, SEYBERT, 2003). After this, the validated FEA was extended for a tapered side outlet muffler. The transmission losses of both mufflers are compared and a gain of 8.96 dB is observed in the case of the tapered side outlet muffler. The transmission loss curve, acoustic pressure level contours, and sound pressure level contours are presented and discussed. The contours confirm the excitation of higher-order modes inside the tapered side outlet muffler above the cut-off frequency.

2. Analytical modelling for the side outlet muffler

The analytical modelling of a side outlet muffler requires pressure equation, particle velocity equation, transfer matrices, characteristic impedance, etc. In the first part, a generalized procedure is presented for a muffler system with $N + 1$ components for its transmission loss formulation. In the second part, the expression for transmission loss of the side outlet muffler is evaluated.

2.1. Transmission loss for muffler system with $N + 1$ components

The formulation for the transmission loss of muffler requires the equation of pressure and equation of particle velocity of sound waves. Let the muffler system consists of $N+1$ components as shown in Fig. 1. The direction of wave propagation is from left to right. The extreme of the left side is the inlet and the extreme of the right side is the outlet of the muffler. The pressure of the wave at the inlet of the muffler is the combined outcome of the incident wave and the reflected wave. The pressure of the wave at the outlet is the result of the incident wave only. It is because of the assumption of anechoic termination at the outlet of the muffler.
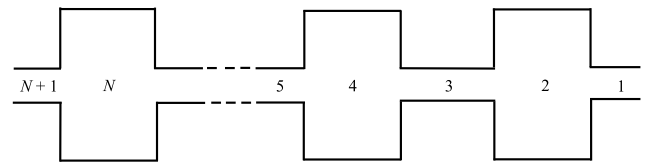

Fig. 1. A muffler system with its components.

The pressure distribution (LEE *et al.*, 2019) for a one-dimensional propagating wave is:

$$P(x) = A_{N+1} \cdot e^{-ikx} + B_{N+1} \cdot e^{ikx}, \qquad (1)$$

where A_{N+1} and B_{N+1} are the coefficients of the incident wave and reflected wave, $i = \sqrt{-1}$, k is a wavenumber (ratio of angular velocity and speed of sound), and x is the direction of wave propagation. The particle velocity for a one-dimensional propagating wave can be achieved by the ratio of pressure and impedance. The particle velocity (LEE *et al.*, 2019) for the wave can be given by:

$$v(x) = \frac{A_{N+1} \cdot e^{-ikx} - B_{N+1} \cdot e^{ikx}}{\rho \cdot c}, \qquad (2)$$

where ρ (1.225 kg/m^3) and c (343 m/s) are the density (medium is air) and velocity of sound in the medium, respectively. Mostly, mass velocity is used for this kind of study. Hence, mass velocity can be written as:

$$V(x) = \frac{A_{N+1} \cdot e^{-ikx} - B_{N+1} \cdot e^{ikx}}{Y}, \qquad (3)$$

where $Y = c/S$ (known as characteristic impedance), S is the area of the cross-section perpendicular to the wave direction. At the inlet of the muffler, pressure is the combined effect of the incident wave and reflected wave. Therefore, pressure and mass velocity at the inlet can be written as (MUNJAL, 1987):

$$P_{N+1} = A_{N+1} + B_{N+1}, \tag{4}$$

$$V_{N+1} = \frac{A_{N+1} - B_{N+1}}{Y_{N+1}}. \tag{5}$$

At the entry of the outlet of the muffler, there is no reflected wave and hence pressure and velocity equation can be written as (MUNJAL, 1987):

$$P_1 = A_1, \tag{6}$$

$$V_1 = P_1/Y_1. \tag{7}$$

The variables (sound pressure and volume velocity) at the inlet can be related to the outlet with the help of the transfer matrix **T**. The parameters P_{N+1}, P_1, V_{N+1}, V_1 are the sound pressure at the inlet, sound pressure at the outlet, volume velocity at the inlet, and volume velocity at the outlet respectively. The relation can be given as:

$$\begin{bmatrix} P_{N+1} \\ V_{N+1} \end{bmatrix} = \begin{bmatrix} T_{11} & T_{12} \\ T_{21} & T_{22} \end{bmatrix} \begin{bmatrix} P_1 \\ V_1 \end{bmatrix}. \tag{8}$$

From the given overall transfer matrix, one can relate the pressure and velocity at the inlet and outlet with the components of the transfer matrix:

$$P_{N+1} = T_{11} \cdot P_1 + T_{12} \cdot V_1, \tag{9}$$

$$V_{N+1} = T_{21} \cdot P_1 + T_{22} \cdot V_1. \tag{10}$$

By using the boundary conditions at inlet and outlet in Eqs (9) and (10), relations among the coefficients of the incident waves, reflected waves, and characteristic impedance can be established:

$$A_{N+1} + B_{N+1} = T_{11} \cdot A_1 + T_{12} \cdot \frac{A_1}{Y_1}, \tag{11}$$

$$A_{N+1} - B_{N+1} = Y_{N+1} \cdot \left\{ T_{21} \cdot A_1 + T_{22} \cdot \frac{A_1}{Y_1} \right\}. \tag{12}$$

A_{N+1} and B_{N+1} can be obtained from Eqs (11) and (12). The transmission loss (MUNJAL, 1987) can be written as:

$$\mathrm{TL} = 20 \cdot \log \left\{ \frac{A_{N+1}}{A_1} \right\}. \tag{13}$$

2.2. Transmission loss for simple expansion chamber with axial inlet and side outlet

The transmission loss of the acoustic muffler can be enhanced by incorporating changes in its design. Side outlet configuration in the expansion chamber increases the transmission loss of the muffler. Figure 2a shows the position of the outlet in the expansion chamber. The outlet is perpendicular to the inlet of the muffler.
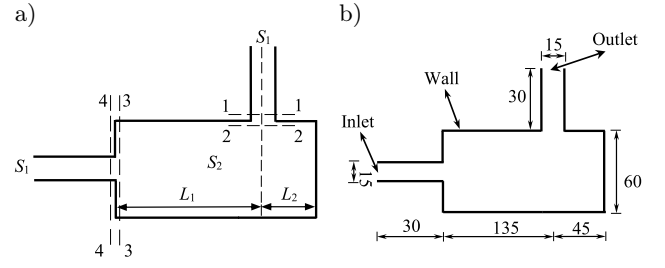

Fig. 2. Simple expansion chamber having side outlet: a) with stations, b) with dimensions (ZHANG *et al.*, 2020); all dimensions are in mm.

The S_1 and S_2 are the cross-sectional areas of the inlet/outlet and expansion chamber of the muffler, respectively. L_1 is the length of the expansion chamber up to the centre of the outlet and L_2 is the length from the centre of the outlet to the end of the expansion chamber. The 2×2 transfer matrix for this configuration is given by (ZHANG *et al.*, 2020):

$$\mathbf{T} = \begin{bmatrix} a^* - b^* \cdot c^* & i \cdot Y' \cdot b^* \\ \dfrac{i}{Y'} \cdot \{ b^* + a^* \cdot c^* \} & a^* \end{bmatrix}, \tag{14}$$

where

$$a^* = \cos(kL_1), \quad b^* = \sin(kL_1), \quad c^* = \tan(kL_2),$$

and Y' is the characteristic impedance of the expansion chamber of muffler. From Eqs (11) and (12) one can get:

$$A_{N+1} + B_{N+1} = \cos(kL_1) - \sin(kL_1) \cdot \tan(kL_2) \cdot A_1$$
$$+ i \cdot Y' \cdot \sin(kL_1) \cdot \frac{A_1}{Y_1}, \tag{15}$$

$$A_{N+1} - B_{N+1} = \frac{i}{Y'} \cdot Y_{N+1}$$
$$\cdot \{ \sin(kL_1) + \cos(kL_1) \cdot \tan(kL_2) \}$$
$$\cdot A_1 + \cos(kL_1) \cdot A_1, \tag{16}$$

where $Y_{N+1} = Y_1$ is the characteristic impedance of the inlet/outlet. Equations (15) and (16) can be used to find the ratio of A_{N+1} and A_1. Replacing $\cos(kL_1)$, $\sin(kL_1)$, and $\tan(kL_2)$ with P, Q, and R, respectively:

$$\frac{A_{N+1}}{A_1} = P - \frac{1}{2} \cdot Q \cdot R + \frac{i}{2} \cdot Q \left(\frac{Y_1}{Y'} + \frac{Y'}{Y_1} \right)$$
$$+ i \cdot \frac{Y_1}{Y'} \cdot \frac{1}{2} \cdot P \cdot R, \tag{17}$$

$$\mathrm{TL} = 20 \cdot \log \left\{ P - \frac{1}{2} \cdot Q \cdot R + \frac{i}{2} \cdot Q \left(\frac{Y_1}{Y'} + \frac{Y'}{Y_1} \right) \right.$$
$$\left. + i \cdot \frac{Y_1}{Y'} \cdot \frac{1}{2} \cdot P \cdot R \right\}. \tag{18}$$

Equation (18) gives the expression for transmission loss of side outlet muffler configuration.

3. Acoustic modelling

The acoustics analysis of the side outlet muffler is done in the ANSYS workbench (student version). The acoustic analysis of the muffler is carried out in the harmonic acoustics module. In acoustic modelling, Navier-Stokes equations of fluid momentum and the flow continuity equations are used for the formulation of acoustic wave equations (Mechanical APDL [MAPDL]: 2020 R1).

From the law of conservation of mass, the flow continuity equation is:

$$\frac{\partial \rho}{\partial t} = -\nabla \cdot (\rho \mathbf{v}) + Q, \qquad (19)$$

where $\mathbf{v}$, ρ, Q, and t are the velocity vector in the x-, y-, and z-directions, density, mass source [kg/m^{3}t], and time, respectively.

From the law of conservation of momentum, the Navier-Stokes equation is:

$$\rho \frac{d\mathbf{v}}{dt} = -\nabla p + \nabla \cdot \overline{\overline{S}} + \rho \mathbf{b}, \qquad (20)$$

where $\overline{\overline{S}}$, p, and $\mathbf{b}$ are viscous stress tensor, pressure, and body force, respectively.

The fluid momentum (Navier-Stokes) equations and continuity equations are simplified to get the acoustic wave equation with certain assumptions like compressible and irrotational fluid medium, absence of body forces, small pressure disturbance of the fluid medium, and no mean flow of the fluid.

The linearized continuity equation is:

$$\nabla \cdot \mathbf{v}_a = -\frac{1}{\rho c^2} \frac{\partial^2 p_a}{\partial t^2} + \frac{Q}{\rho}. \qquad (21)$$

The linearized Navier-Stokes equation is:

$$\frac{\partial \mathbf{v}_a}{\partial t} = -\frac{1}{\rho} \nabla p_a + \frac{4}{3} \frac{\mu}{\rho} \nabla \left(-\frac{1}{\rho c^2} \frac{\partial p_a}{\partial t} + \frac{Q}{\rho} \right), \qquad (22)$$

where $\mathbf{v}_a$, p_a, c, and μ are the acoustic velocity, acoustic pressure, speed of sound, and dynamic viscosity of the medium, respectively.

From Eqs (21) and (22) acoustic wave equation can be formulated as:

$$\nabla \cdot \left(\frac{1}{\rho} \nabla p_a \right) - \frac{1}{\rho c^2} \frac{\partial^2 p_a}{\partial t^2} + \nabla \cdot \left[\frac{4}{3} \frac{\mu}{\rho} \nabla \left(\frac{1}{\rho c^2} \right) \frac{\partial p_a}{\partial t} \right]$$

$$= -\frac{\partial}{\partial t} \left(\frac{Q}{\rho} \right) + \nabla \cdot \left[\frac{4}{3} \frac{\mu}{\rho} \nabla \left(\frac{Q}{\rho} \right) \right]. \quad (23)$$

Initially, the side outlet muffler has been simulated using FEA. The validated FEA is then extended for a tapered side outlet muffler.

3.1. Side outlet muffler

The geometry of the side outlet muffler is created in the design modular of the workbench. The outlet of the muffler is perpendicular to the inlet which is shown in Fig. 2b. The diameters of the inlet pipe, expansion chamber, and outlet pipe are 15 mm, 60 mm, and 15 mm, respectively. The lengths of the inlet pipe, expansion chamber, and outlet pipe are 30 mm, 180 mm, and 30 mm, respectively. The flow domain for the sound propagation is discretized into FLUID221 tetrahedral (10-node acoustic solid) elements. The range of frequency of analysis is from 0 Hz to 4000 Hz. The grid size (6 divisions per wavelength) is selected based on the maximum frequency of interest. The grid independency test is done by varying the grid size. The parameter considered for the grid independency test is the transmission loss of the muffler. A grid size of 7.5 mm with 10897 tetrahedral elements is chosen for the acoustics analysis.

The radiation boundary condition is applied at the inlet and outlet of the muffler. The radiation boundary condition takes care of the anechoic termination. The surface velocity condition is applied at the inlet of the muffler to create the source of the disturbance in the medium. The surface velocity is taken as 10 m/s. The walls of the domain are set to the rigid wall to apply the Neumann boundary conditions. Ports are defined to calculate the transmission loss of the muffler.
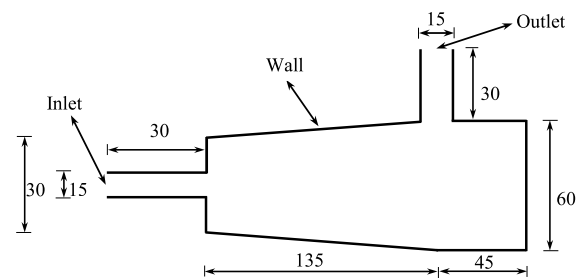

Fig. 3. Computational flow domain of tapered side outlet muffler, all dimensions are in mm.

3.2. Tapered side outlet muffler

The modification is proposed in the shape of the expansion chamber of the side outlet muffler to increase the transmission loss of the muffler. The plane wave analysis of the tapered expansion chamber muffler (VISHWAKARMA, PAWAR, 2021) is the basis for this modification. The details of the dimensions of the tapered side outlet muffler are given in Fig. 4. The diameter of the expansion chamber is varied from 30 mm to 60 mm within a length of 135 mm till the centre of the outlet.

The remaining length of the expansion chamber has a constant diameter of 60 mm. The dimensions of the inlet and outlet pipes remain the same. The centre of
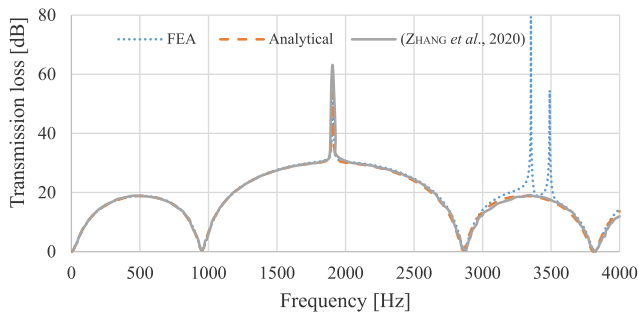
Fig. 4. Comparison of transmission loss of side outlet muffler.

the outlet pipe is 45 mm from the end of the expansion chamber. The proposed muffler is examined using the same boundary conditions as those described previously. A grid size of 3.8 mm with 55 280 tetrahedral elements is selected for the simulation.

4. Results and discussion

The transmission loss obtained from the analytical modelling of the side outlet muffler is shown with a light orange coloured dashed line, from Zhang et al. (2020) is shown with a grey coloured solid line, and from FEA is shown with a light blue coloured dotted line (Fig. 4). There is an excellent match of curves obtained from analytical modelling, FEA, and (Zhang et al., 2020). After careful observation, it is found that results deviate from each other by a very minute amount at each frequency which can be ignored. The values of maximum transmission loss obtained from analytical modelling and (Zhang et al., 2020) are 62.70 dB at 1907 Hz, and 62.71 dB at 1907 Hz, respectively, with a maximum percentage error of 0.016%. It indicates that the analytical modelling of the side outlet muffler is valid and can be extended for the other mufflers. The FEA curve shows fair agreement with (Zhang et al., 2020) up to the cut-off frequency (Munjal, 1987) of the muffler. The cut-off frequency of the side outlet muffler comes out to be 3349.89 Hz. The maximum value of transmission loss of the side outlet muffler from FEA is 62.83 dB at 1909 Hz. The percentage error between transmission losses from FEA with (Zhang et al., 2020) is 0.19% and with analytical modelling is 0.21%. This comparison validated the FEA of the side outlet muffler with Zhang et al. (2020). The FEA curve has two abrupt peaks above the cut-off frequency. The frequencies of the two abrupt peaks are 3353 Hz and 3490 Hz. The reason behind this is the excitation of the higher-order modes (Falin et al., 2010; Mimani, Munjal, 2012) which represent the pressure variation in the transverse plane (Munjal, 1987). The plane wave corresponds to the $(0, 0)$ mode of the wave. The higher modes can be of the type $(0, 1)$, $(1, 0)$, etc. There is no abrupt peak in the analytical curve of the side outlet muffler because

it is based on the assumption of plane wave analysis and it does not account for the effect of higher-order modes.

The FEA model is also validated with the work by Tao and Seybert (2003) on simple expansion chamber muffler. The frequency range in this study is from 0 Hz to 3000 Hz. The comparison of transmission loss of simple expansion chamber muffler obtained from the FEA with the experimental work by Tao and Seybert (2003) is shown in Fig. 5. There is an excellent match of transmission loss curves throughout the entire frequency range. The matching of curves indicates the feasibility of the FEA model for the reactive mufflers.
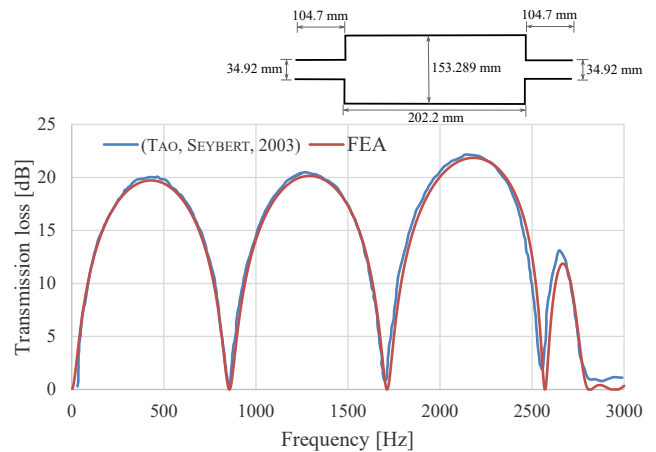

Fig. 5. Comparison of transmission loss of simple expansion chamber muffler.

The comparison of the transmission losses of the side outlet muffler (dotted blue coloured line) and the tapered side outlet muffler (solid orange coloured line) is presented in Fig. 6. The FEA of the side outlet muffler and tapered side outlet muffler is done using the same boundary conditions. In the first one-third of the frequency range (from 0 Hz to 1333 Hz), it can be seen that the tapered side outlet muffler has a wide (from 0 Hz to 1049 Hz) working frequency range as compared to the side outlet muffler (from 0 Hz to 955 Hz). The performance of the side outlet muffler is
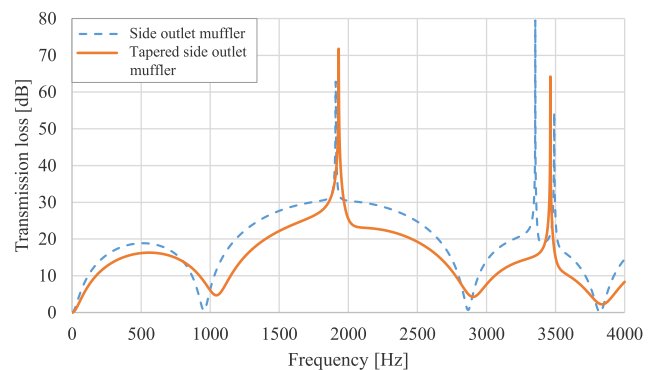

Fig. 6. Comparison of FEA of side outlet muffler and tapered side outlet muffler.

better than the tapered side outlet muffler in the frequency range from 0 Hz to 806 Hz. The tapered side outlet muffler shows better performance in the frequency range from 807 Hz to 1000 Hz. The first peak values in the transmission loss curves of the side outlet muffler and tapered side outlet muffler are 18.86 dB at 508 Hz and 16.29 dB at 563 Hz, respectively. The first trough values in the transmission loss curves of the side outlet muffler and tapered side outlet muffler are 0.52 dB at 955 Hz and 4.69 dB at 1045 Hz. In the 1334 Hz to 2905 Hz frequency range, the side outlet muffler has a wider working frequency range (955–2867 Hz) as compared to the tapered side outlet muffler (1045–2903 Hz).

The second trough values in the transmission loss curves of the side outlet muffler and tapered side outlet muffler are 0.70 dB at 2867 Hz and 4.26 dB at 2903 Hz. The comparison of the trough values in the transmission loss curves indicates that the tapered side outlet muffler has a better ability in noise suppression. The side outlet muffler shows the peak of transmission loss at 1909 Hz whereas, for the tapered side outlet muffler, it is at 1930 Hz. The maximum transmission loss for the tapered side outlet muffler comes out to be 71.79 dB. The tapered side outlet muffler shows a better response to higher-order modes of the sound wave

as there is only one abrupt peak (at 3462 Hz) in the transmission loss, whereas the side outlet muffler has two abrupt peaks (at 3353 Hz and 3490 Hz). There is also a decrement in the transmission loss value at the abrupt peak. The reason behind the suppression of the peak is the tapered section of the muffler. There is a continuous change in the characteristic impedance of the tapered side outlet muffler along the length of the muffler because of the varying area section in the expansion chamber.

The acoustic pressure contours of the tapered side outlet muffler at different frequencies are shown in Fig. 7. The contours are shown at 563 Hz, 1930 Hz, 3349 Hz, and 3462 Hz frequencies. The 563 Hz and 1930 Hz are the frequencies for the maximum transmission loss of the tapered side outlet muffler below the cut-off frequency. The frequencies such as 3349 Hz and 3462 Hz are the cut-off frequency, and maximum transmission loss frequency for higher-order modes, respectively. The low-frequency sound waves produce lower acoustic pressure, whereas the high-frequency sound waves produce higher acoustic pressure. The maximum acoustic pressures at 563 Hz, 1930 Hz, 3349 Hz, and 3462 Hz are 1531.5 Pa, 6768.2 Pa, 7572.8 Pa, and 6935.2 Pa, respectively. The first three acoustic pressure values are for plane waves, but the fourth acoustic
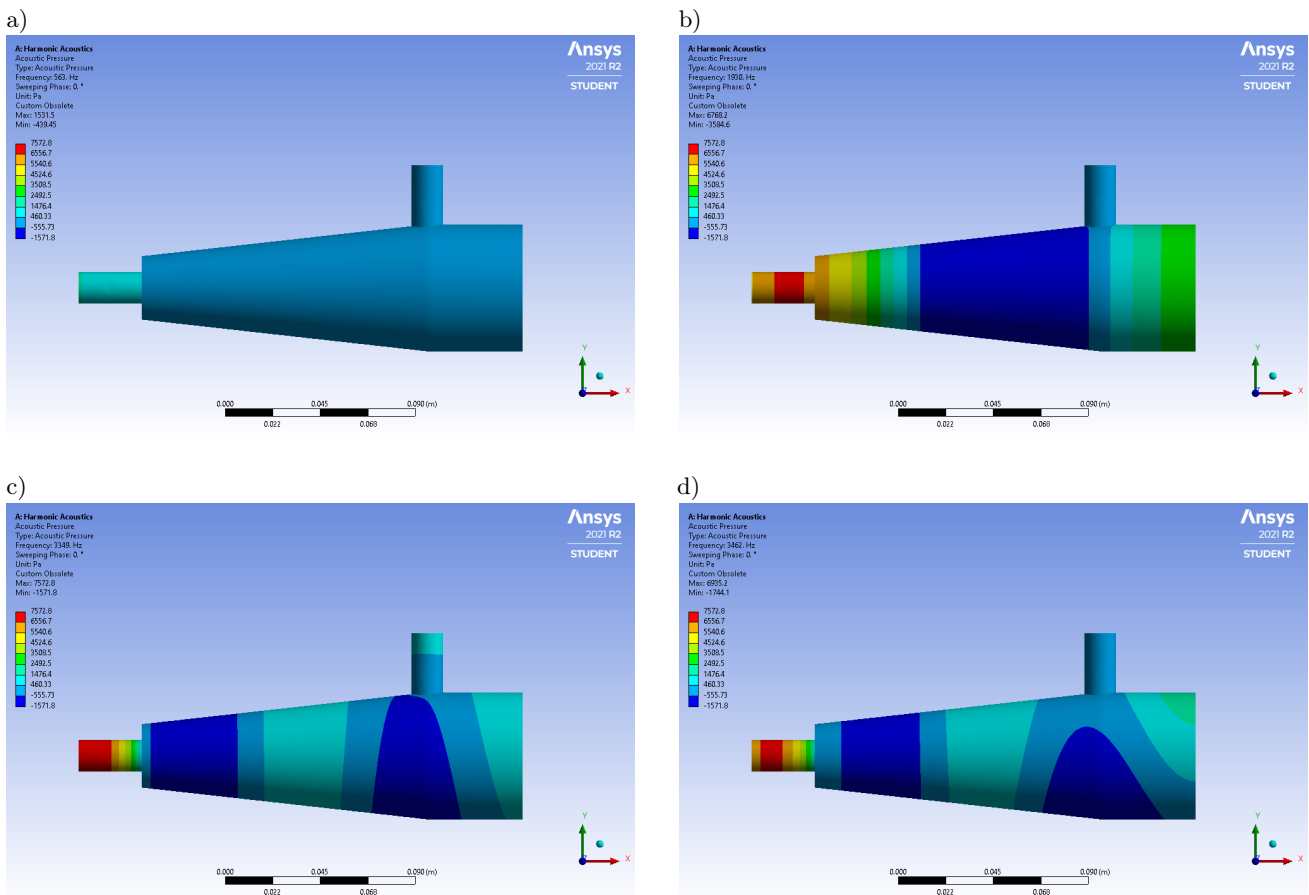

Fig. 7. Acoustic pressure contours at: a) 563 Hz, b) 1930 Hz, c) 3349 Hz, d) 3462 Hz.

pressure value is for non-planar waves. The acoustic pressure value at 3462 Hz is lower than the previous value because of the transverse distribution of the pressure of the higher-order mode. The transmission loss, acoustic pressure values, and sound pressure values at the above frequencies are listed in Table 1.

The sound pressure level contours at the above four frequencies are shown in Fig. 8. The sound pressure level is the most commonly used indicator of acoustic wave strength. The red and blue colour bands are for the maximum and minimum sound pressure levels inside the muffler. The acoustic wave strength is varying along the length of the tapered side outlet muffler. This happens because of the impedance mismatch phenomenon. The sound pressure level contours are different for different frequencies of the sound wave. The transmission loss of the tapered side outlet muf-

fler is maximum at 1930 Hz, Fig. 8b shows the variation of sound pressure level at this frequency. The maximum and minimum sound pressure at this frequency is 169.46 dB and 62.99 dB, respectively. The 169.46 dB is at the inlet and 62.99 dB is at the outlet of the tapered side outlet muffler. The variation of sound pressure level inside the muffler at the four mentioned frequencies indicates that the tapered side outlet muffler is best effective for the sound wave with frequencies near 1930 Hz.

The transmission loss curve, acoustic pressure contours, and sound pressure level contours for the tapered side outlet muffler in the 0–4000 Hz are presented in Figs 6–8, respectively. This range of frequency is chosen to analyse the effect of higher order modes on the transmission loss of the muffler. Through the careful observation of the curve and contours, it is found that

Table 1. Variation of transmission loss, acoustic pressure, and sound pressure level with frequency.

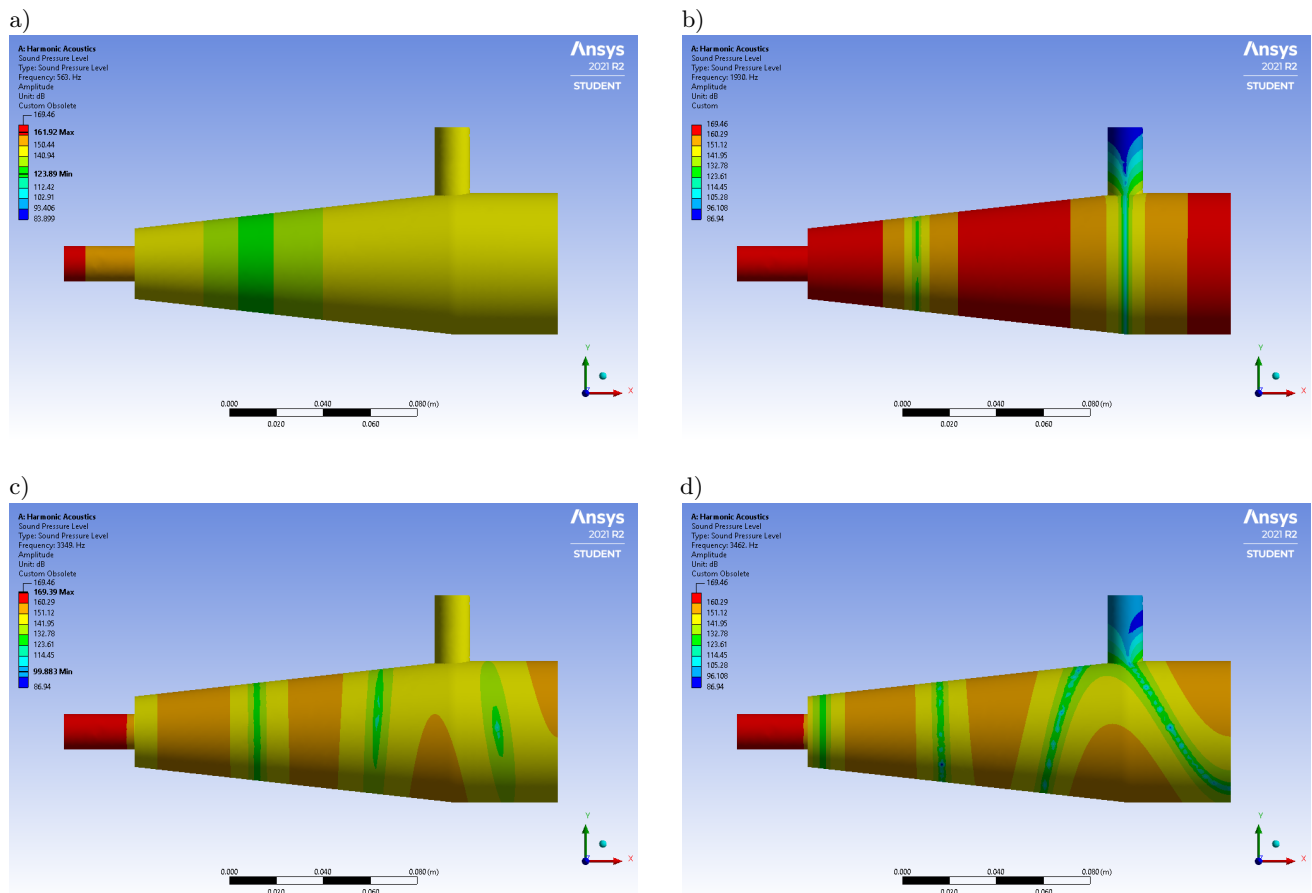| Variables/Frequencies		563 Hz	1909/1930 Hz	3349 Hz	3462 Hz
Transmission loss [dB]	Side outlet muffler	18.74	62.83 at 1909 Hz	36.74	21.34
	Tapered side outlet muffler	16.29	71.79 at 1930 Hz	15.37	64.22
Acoustic pressure [Pa]		1531.5	6768.2	7572.8	6935.2
Maximum Sound pressure level [dB]		161.92	169.46	169.39	169.46
Minimum Sound pressure level [dB]		123.89	86.94	99.88	86.94

Fig. 8. Sound pressure levels at: a) 563 Hz, b) 1930 Hz, c) 3349 Hz, d) 3462 Hz.

the tapered side outlet muffler is effective for the 807–1000 Hz or 1915–1966 Hz frequency sound waves. The application of the mufflers in the automobiles depends upon the type of internal combustion engine used in the automobiles. An optimized designed muffler should be working to dampen the sound wave over some range of frequency, which in turn is parallel to speed of the engine. The speed of the engine also determine the velocity of flow of the exhaust gases inside the muffler. The fluid-structure interaction has been not considered in this study. The side outlet mufflers are most commonly used in Nitro-racing cars. The proposed tapered side outlet muffler can reduce the noise from the engine of Nitro-racing cars effectively as compared to the side outlet muffler.

5. Conclusions

The analytical modelling and acoustic modelling (using FEA) of the side outlet muffler were done and the performance of the muffler in terms of transmission loss is compared with the Zhang *et al.* (2020). The analytical modelling and FEA replicate the transmission loss of the side outlet muffler with fair accuracy. The percentage errors found in the above two modelling in comparison with the Zhang *et al.* (2020) are 0.016% and 0.19%. After the validation of the FE model, it was extended for the tapered side outlet muffler. The shape of the expansion chamber of the tapered side outlet muffler is made tapered up to 135 mm in length. The variation of diameters of the expansion chamber is from 30 mm (at starting) to 60 mm (at the end). The remaining length (45 mm) of the expansion chamber has a constant diameter of 60 mm. This modification leads to the better performance of the muffler.

The tapered side outlet muffler has effectiveness in the 0 Hz to 1049 Hz frequency range which is wider than the side outlet muffler (0 Hz to 955 Hz). The transmission loss of the tapered side outlet muffler is 8.96 dB more than the side outlet muffler. Also, due to a change in the shape of the expansion chamber, there is a shift in the frequency of sound for the maximum transmission loss. The tapered side outlet muffler is effective for a sound wave with frequencies near 1930 Hz. The acoustic pressure level and sound pressure level contours inside the tapered side outlet muffler are evaluated at 563 Hz, 1930 Hz, 3349 Hz, and 3462 Hz. There is plane wave propagation inside the tapered side outlet muffler below 3349 Hz (cut-off frequency). The acoustic pressure levels at the frequencies below 3349 Hz are clearly showing the presence of plane waves only. But above the cut-off frequency, the higher-order modes start to propagate. At 3462 Hz, there is a decrement in the acoustic pressure level due to the transverse pressure distribution of higher-order modes. The acoustic wave strength can be seen from the sound pressure level contours. The sound pressure

level contours also confirm the excitation of non-planar sound waves above the cut-off frequency. This study offers the advantage in the prediction of the transmission loss of the mufflers. The side outlet mufflers save space and improve muffler performance. This muffler is effective for the engines where the frequency of sound waves is of the order of 800–1000 Hz or 1915–1966 Hz.

Acknowledgments

References

1. Åbom M. (1990), Derivation of four pole parameters including higher order mode effects for expansion chamber mufflers with extended inlet and outlet, *Journal of Sound and Vibration*, **137**(3): 403–418, doi: 10.1016/0022-460X(90)90807-C.

2. Banerjee S., Jacobi A.M. (2013), Transmission loss analysis of single-inlet/double-outlet (SIDO) and double-inlet/single-outlet (DISO) circular chamber mufflers by using Green's function method, *Applied Acoustics*, **74**(12): 1499–1510, doi: 10.1016/j.apacoust.2013.06.007.

3. Banerjee S., Jacobi A.M. (2015), Analytical prediction of transmission loss in distorted circular chamber mufflers with extended inlet/outlet ports by using a regular perturbation method, *Journal of Vibration and Acoustics*, **137**(6): 061002, doi: 10.1115/1.4030717.

4. Barbieri R., Barbieri N. (2006), Finite element acoustic simulation based shape optimization of a muffler, *Applied Acoustics*, **67**(4): 346–357, doi: 10.1016/j.apacoust.2005.06.007.

5. Bilawchuk S., Fyfe K.R. (2003), Comparison and implementation of the various numerical methods used for calculating transmission loss in silencer systems, *Applied Acoustics*, **64**(9): 903–916, doi: 10.1016/S0003-682X(03)00046-X.

6. Craggs A. (1989), The application of the transfer matrix and matrix condensation methods with finite elements to duct acoustics, *Journal of Sound and Vibration*, **132**(3): 393–402, doi: 10.1016/0022-460X(89)90633-0.

7. Chang Y.-C., Chiu M.-C. (2010), Optimization of multi-chamber mufflers with reverse-flow ducts by algorithm of simulated annealing, *Archives of Acoustics*, **35**(1): 13–33.

8. Chang Y.-C., Chiu M.-C., Wu M.-R. (2018), Acoustical assessment of automotive mufflers using FEM, neural networks, and a genetic algorithm, *Archives of Acoustics*, **43**(3): 517–529, doi: 10.24425/123923.

9. Chang Y.-C., Yeh L.-J., Chiu M.-C. (2004), GA optimization on single-chamber muffler hybridized with

extended tube under space constraints, *Archives of Acoustics*, **29**(4): 577–596.

10. Chiu M.-C. (2011), Optimization design of hybrid mufflers on broadband frequencies using the genetic algorithm, *Archives of Acoustics*, **36**(4): 795–822, doi: 10.2478/v10168-011-0053-5.

11. Falin Z., Dehua L., Yuping Z. (2010), Effect of higher order modes on muffler performance, [in:] *International Conference on Optoelectronics and Image Processing*, pp. 468–472, Haikou, China, doi: 10.1109/ICOIP.2010.70.

12. Kagawa Y., Omote T. (1976), Finite element simulation of acoustic filters of arbitrary profile with circular cross-section, *The Journal of the Acoustical Society of America*, **60**(5): 1003–1013, doi: 10.1121/1.381199.

13. Kani M. *et al.* (2019), Acoustic performance evaluation for ducts containing porous materials, *Applied Acoustics*, **147**(1): 15–22, doi: 10.1016/j.apacoust.2018.08.002.

14. Keskar H., Venkatesham B. (2017), Transmission loss characteristics of an annular cavity with arbitrary port locations using Green's function method, *The Journal of the Acoustical Society of America*, **142**(3): 1350–1361, doi: 10.1121/1.5001492.

15. Kuskinen C., Riveros A., Floody S. (2010), Shape optimization of reactive-dissipative mufflers, *The Journal of the Acoustical Society of America*, **128**(1): 2367, doi: 10.1121/1.3508404.

16. Lamancusa J. (1988), The transmission loss of double expansion chamber mufflers with unequal size chambers, *Applied Acoustics*, **24**(1): 15–32, doi: 10.1016/0003-682X(88)90068-0.

17. Lee J.K., Oh K.S., Lee J.W. (2019), Methods for evaluating in-duct noise attenuation performance in a muffler design problem, *Journal of Sound and Vibration*, **464**: 114982, doi: 10.1016/j.jsv.2019.114982.

18. Mechanical APDL: 2020 R1, *Acoustics – Acoustic Fundamental (Ch. 8), ANSYS workbench help documentation, release 2020 R1*, https://d.shikey.com/down/Ansys.Products.2020.R1.x64/install_docs/Ansys.Products.PDF.Docs.2020R1/v201/ANSYS_Mechanical_APDL_Theory_Reference.pdf (access: 28.08.2022).

19. Mimani A., Munjal M.L. (2012), 3-D acoustic analysis of elliptical chamber mufflers having an end-inlet and a side-outlet: An impedance matrix approach, *Wave Motion*, **49**(2): 271–295, doi: 10.1016/j.wavemoti.2011.11.001.

20. Mimani A., Munjal M.L. (2016), Design of reactive rectangular expansion chambers for broadband acoustic attenuation performance based on optimal port location, *Acoustics Australia*, **44**(2): 299–323, doi: 10.1007/s40857-016-0053-8.

21. Munjal M.L. (1975), Velocity ratio-cum-transfer matrix method for the evaluation of a muffler with mean flow, *Journal of Sound and Vibration*, **39**(1): 105–119, doi: 10.1016/S0022-460X(75)80211-2.

22. Munjal M.L. (1987), *Acoustics of duct and mufflers with application to exhaust and ventilation system*, John Wiley and Sons, New York.

23. Perrey-Debain E., Marechal R., Ville J.M. (2014), Side-branch resonators modelling with Green's function methods, *Journal of Sound and Vibration*, **333**(19): 4458–4472, doi: 10.1016/j.jsv.2014.04.060.

24. Saharabudhe A.D., Ramu S.A., Munjal M.L. (1991), Matrix condensation and transfer matrix techniques in the 3-D analysis of expansion chamber mufflers, *Journal of Sound and Vibration*, **147**(3): 371–394, doi: 10.1016/0022-460X(91)90487-5.

25. Selamet A., Ji Z.L. (1998), Acoustic attenuation performance of circular expansion chambers with offset inlet/outlet: I. Analytical approach, *Journal of Sound and Vibration*, **213**(4): 601–617, doi: 10.1006/jsvi.1998.1514.

26. Seybert A.F., Cheng C.Y.R. (1987), Application of the boundary element method to acoustic cavity response and muffler analysis, *Journal of Vibration, Acoustics, Stress, and Reliability in Design*, **109**(1): 15–21, doi: 10.1115/1.3269388.

27. Suwandi D., Middelberg J., Byrne K.P., Kessissoglou N.J. (2005), Predicting the performance of mufflers using transmission line theory, [in:] *Proceedings of ACOUSTICS*, pp. 181–187.

28. Tao Z., Seybert A.F. (2003), A review of current techniques for measuring muffler transmission loss, *SAE Technical Paper Series*, pp. 1–5, doi: 10.4271/2003-01-1653.

29. To C.W.S. (1984), The acoustic simulation and analysis of complicated reciprocating compressor piping systems, I: Analysis technique and parameter matrices of acoustic elements, *Journal of Sound and Vibration*, **96**: 175–194, doi: 10.1016/0022-460X(84)90577-7.

30. Vishwakarma S.K., Pawar S.J. (2021), Simulation studies on the transition from simple expansion chamber muffler to tapered expansion chamber muffler, [in:] *Advances in Fluid and Thermal Engineering*, Sikarwar B.S., Sundén B., Wang Q. [Eds], pp. 389–398, Springer Nature Singapore, doi: 10.1007/978-981-16-0159-0_34.

31. Wu T.W., Wan G.C. (1996), Muffler performance studies using a direct mixed-body boundary element method and a three-point method for evaluating transmission loss, *Journal of Vibration and Acoustics*, **118**(3): 479–484, doi: 10.1115/1.2888209.

32. Wu T.W., Zhang P., Cheng C.Y.R. (1998), Boundary element analysis of mufflers with an improved method for deriving the four-pole parameters, *Journal of Sound and Vibration*, **217**(4): 767–779, doi: 10.1006/jsvi.1998.1800.

33. Young C.I.J., Crocker M.J. (1975), Prediction of transmission loss in mufflers by the finite element method, *The Journal of the Acoustical Society of America*, **57**(1): 144–148, doi: 10.1121/1.380424.

34. Zhang L., Shi H.M., Zeng X.H., Zhuang Z. (2020), Theoretical and experimental study on the transmission loss of a side outlet muffler, *Journal of Shock and Vibration*, 6927574, doi: 10.1155/2020/6927574.